Available online at www.sciencedirect.com
ScienceDirect
Journal of Electroanalytical Chemistry 611 (2007) 208–216
Journal of Electroanalytical Chemistry
www.elsevier.com/locate/jelechem

Electric field assisted nanocolloidal gold deposition

E. Stefan Kooij *, E.A. Martijn Brouwer, Bene Poelsema

Solid State Physics group, MESA+ Institute for Nanotechnology, University of Twente, P.O. Box 217, 7500AE Enschede, The Netherlands

Received 9 May 2007; received in revised form 29 August 2007; accepted 31 August 2007
Available online 7 September 2007

Abstract

The deposition of nanocolloidal gold particles under the influence of an externally applied electric field is studied in situ by means of spectroscopic ellipsometry. The variation of the relative coverage with time, as a function of applied potential, is determined using a principal component analysis. Calibration of the absolute coverage is done by means of ex situ electron microscopy. The results reveal that the deposition rate is directly related to the electrochemical current. A threshold potential exists for current and therewith also deposition to occur. The spatial distribution of nanoparticles deposited in an applied field exhibits a higher degree of order as compared to the random, irreversibly deposited nanocolloids at chemically functionalized surfaces. The experimental findings are discussed in terms of a simple electrochemical model.

PACS: 78.67.Bf; 81.15.Pq; 81.16.Dn; 82.45.Yz

Keywords: Nanocolloidal gold; Particle adsorption; Spectroscopic ellipsometry; Electrophoretic deposition

1. Introduction

During the past decade, impressive and promising advancements have been reported in the field of bottom-up self-assembly. Despite recent achievements, true control over the formation of single and multicomponent arrays still remains one of the 'holy grails' and is pursued by many groups. For example, electrostatically driven self-assembly and chemically oriented routes to self-organization of nanoparticles, employing well-defined functionalities to induce specific affinity between composing entities, have been studied extensively [1–3].

In recent work, we have shown that nanoparticle deposition driven by electrostatic attraction between particles in suspension and a chemically charged substrate results in randomly deposited colloidal thin films [4,5]. Due to the irreversibility of the adsorption process, the resulting films show short-ranged local ordering in the radial direction, but azimuthal ordering is absent. Particles remain well-separated as a result of the electrostatic double layer repulsion, implying that the surface coverage remains limited. For a number of envisaged applications a higher coverage and a more ordered spatial distribution of the particles would be desirable.

Well-ordered multilayered superstructures and ordered monolayer films, prepared by electrophoretic deposition of micron-sized latex particles, were reported almost simultaneously by Trau and co-workers [6] and Böhmer [7]. Since then, considerable effort has been devoted to electrophoretic deposition of (sub)micrometer sized colloidal particles. Highly ordered structures such as three-dimensional colloidal crystals (opals) [8–10] and ordered two-dimensional films of a binary mixture of colloids [11] have been described in literature. The driving force for self-assembly in these systems has been investigated [6,8,11–13] and is generally ascribed to electrohydrodynamic flow [12–16]. Electrohydrodynamic flow is caused by movement of ions due to a gradient in the local electrical field, which results from variations in the charge distribution around an adsorbed particle. As the flow is a response to the variations

* Corresponding author. Tel.: +31 53 489 3146.
E-mail address: e.s.kooij@utwente.nl (E.S. Kooij).
URL: ssp.tnw.utwente.nl (E.S. Kooij).

0022-0728/$ - see front matter © 2007 Elsevier B.V. All rights reserved.
doi:10.1016/j.jelechem.2007.08.023

in the charge density, it only persists if the variations in the charge distribution are maintained, i.e. when an electric current flows.

There are less-frequent reports of electrophoretically deposited films of particles with dimensions in the low-nanometer range. Bailey et al. have shown unordered films deposited by means of electrophoresis on substrates that were pre-patterned using micro contact printing [17]. Another example is from Gao et al. [18], who deposited CdTe nanoparticles on pre-patterned ITO electrodes. Inverse opals made by electrophoretic deposition of small particles into voids left between an ordered multilayer film of large particles have been shown by Gu et al. [10].

Based on the available literature, one can conclude that electric field assisted deposition of nanoparticles has been studied to some extent. Generally, the assembled nanoparticulate films do not exhibit significant ordering. The films deposited by Giersig and Mulvaney [19] constitute the only exception to this rule as far as we are aware. These films show very nice ordering, due to the fact that the particles are mobile even after deposition on the electrode surface. There are a number of factors that make deposition of ordered films of nanoparticles and their investigation more challenging, as opposed to their micron-sized counterparts. First, for aqueous suspensions of nanocolloids, the thickness of the double layer is often comparable to the particle size, giving rise to considerable interparticle repulsion. Second, Brownian motion for small particles is more important than for larger particles, therewith inhibiting ordering of the film. Furthermore, electro-osmotic flow arising from electrophoretic motion of ions in the aqueous liquid near charged surfaces, including the substrate, interferes with the well-defined motion of the charged particles [20]. A last important issue is that nanoparticles can not be observed easily, whereas deposition of larger particles is readily observed using conventional microscopy [6–8,11,13–15].

In this work we describe deposition experiments, in which positively charged gold nanoparticles are deposited under the influence of an externally applied electric field. Spectroscopic ellipsometry [21,22] enables us to monitor the adsorption of nanoparticles in situ, allowing a study of the influence of the applied voltage on the deposition process. Additionally, the spatial distribution of the particles on the electrode is analyzed from electron microscopy images obtained after deposition. Based on the results, a mechanism for electrophoretic deposition from an aqueous suspension is proposed.

2. Experimental

2.1. Nanoparticle synthesis

For the deposition experiments in the presence of an external electric field, octadecylamine stabilized gold particles are used, such as shown in Fig. 1. From the particle size distribution, the average diameter and the polydispersity are determined to amount to 8.6 nm and 13%, respectively.

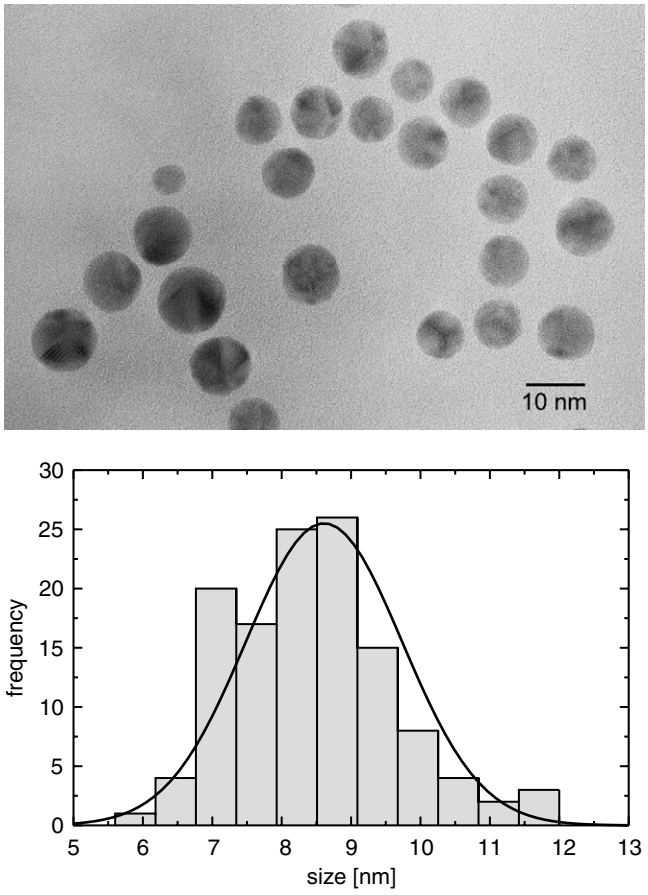

Fig. 1. (top) Transmission electron microscopy (TEM) image showing octadecylamine stabilized gold nanoparticles, as used in this work. (bottom) Size-distribution of the gold nanoparticles yielding an average diameter of 8.6 nm and a standard deviation of 13%.

These particles are synthesized as described by Aslam et al. [23]. Typically, 100 mL of an aqueous solution of 1 mM $HAuCl_4$ (99.999% Aldrich; due to the hygroscopic nature of the solid, it is stored as a stock solution) is heated to 60 °C. Then 190 mg molten octadecylamine is slowly added, resulting in an octadecylamine concentration of 7 mM. Due to the formation of a gold–octadecylamine complex, the solution immediately obtains a bright yellow colour. The temperature is increased to 85 °C. After a few minutes, the solution turns colourless, indicating the reduction of $AuCl_4^-$. After approximately 10 min, a pink colour slowly develops, which indicates that gold colloids are slowly being formed. After 20 more minutes, the solution has the bright dark red colour that is characteristic for gold nanoparticles.

After cooling the solution to room temperature, the particles are precipitated using centrifugation at 20,000 rpm (approximately $45 \times 10^3 g$) for 4 h. The supernatant, containing most of the excess octadecylamine, is discarded and the particles are re-dispersed in ultra-pure water. The octadecylamine concentration is reduced to less than 1‰

of the initial concentration by repeated centrifugation. The resulting concentrated solution can be stored for a few months without noticeable degradation.

As octadecylamine is a weak base, the surface charge of the particles will depend on the pH of the suspension. When hydrogen gas evolves at the cathode, hydroxide ions are produced simultaneously and the pH of the suspension will increase locally. To prevent variation of the surface charge during the experiment, a pH buffer solution is used as background electrolyte. A mixture of sodium benzoate (Sigma) and hydrochloric acid (Merck) with a concentration ratio of 1.65:1 is used to achieve a pH of 4. The concentration of sodium benzoate is typically 10 mM. After adding the hydrochloric acid, the ionic strength is equal to the initial sodium benzoate concentration.

2.2. Substrate and deposition cell

The particles are to be deposited onto a transparent sample that serves as the working electrode. The samples (Ssens) consist of a metal-coated round BK7 glass substrate with a diameter of 25 mm. The coating of the substrate is designed to make the optical transmission (40%) as uniform as possible in the visible range of the spectrum; the outermost layer of the substrate is a gold film with a thickness of 5 nm. Prior to the experiments, samples are cleaned by immersion in an acidic piranha solution (a 2:1 mixture of concentrated H_2SO_4 and H_2O_2), typically for 5–10 s. Atomic force microscopy reveals that the morphology of the surface is not changed. Longer exposure will give rise to enhanced roughness and will eventually lead to dissolution of the metal film. After this treatment, the gold surface is oxidized and consequently has a negative surface charge. Without further treatment of the sample, this surface charge induces an electrostatic attraction between the particles and the substrate, resulting in an uncontrolled deposition process. To prevent this, the surface oxide is reduced by immersing the sample in ethanol for an hour. After cleaning and reduction of the surface, a wire is glued to the sample using a two-component silver epoxy glue. This connecting wire is not in contact with the suspension during the experiment.

A dedicated cell is used for the electric field assisted deposition experiments. A schematic top-view of the cell is shown in Fig. 2. To enable optical access, the sample is mounted on a BK7 glass prism. To prevent optical reflection at the prism-substrate interface, the gap between the substrate and the prism is filled with a refractive index matching fluid (Immersion oil, $n = 1.515$, DIN 58884, Merck). A PTFE (Teflon) coated o-ring with an inner diameter of 14 mm is used to prevent leaking of the suspension, leaving an effective electrode area of 1.5 cm^2. The counter electrode consists of a platinum plate with an area of approximately 1.8 cm^2. The distance between the working and counter electrode can be varied between 0 and 5 mm; typically, the distance amounts to 1–2 mm. A saturated calomel electrode (SCE) is taken as reference; all potentials are given with respect to SCE. This electrode is inserted in a separate compartment, which is connected to the main compartment through a narrow channel. An EG&G Princeton Applied Research PAR-273A potentiostat is used to apply the potential and to measure the current.

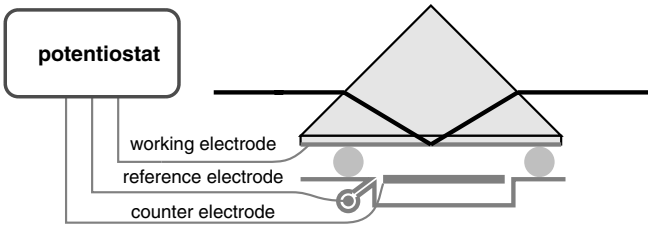

Fig. 2. Schematic top-view representation of the electrochemical cell used to perform in situ spectroscopic ellipsometry during adsorption measurements in the presence of an electric field. A potentiostat is used to apply a field to the working electrode, which consists of a metal film on a glass substrate, as described in the text. Between the substrate and the glass prism, a thin film of immersion oil is present. The light path is indicated by the thick line.

The cell is attached to a sample stage that can be tilted in two directions: (i) around the normal of the triangular sides of the prism enabling fine adjustments of the angle of incidence and (ii) around the normal of the long side of the prism. This construction allows the cell to be aligned for ellipsometry measurements.

2.3. Spectroscopic ellipsometry

In situ monitoring of the electric field assisted deposition is done using a home-built spectroscopic ellipsometer [24,25]. Essential components include a white light source, a monochromator, a detector and two polarizers, one of which continuously rotates [21,22]. In reflection ellipsometry, the change of the polarization state of linearly polarized light is measured upon reflection at an interface. The complex reflection coefficient ρ is defined as

$$\rho = \frac{r_p}{r_s} = \tan(\Psi)\exp(i\Delta) \quad (1)$$

where r_p and r_s are the reflection coefficients for the parallel and perpendicular polarizations, respectively. Historically, the quantity ρ is expressed in the two angles Ψ and Δ [21].

The cell used in the experiments was introduced in the previous section (Fig. 2). We employ a total internal reflection configuration, i.e. the sample is illuminated from the back side through a prism. The incident beam is totally reflected at the substrate-suspension interface, implying a high reflection intensity; the light wave does not propagate into the solution. Adsorbed particles are probed by the exponentially decaying evanescent wave in the suspension. The benefit of this setup is that the gap between the electrodes can be made arbitrarily small. A second advantage is that the measurements are not affected by absorption of the light in the suspension.

In addition to the reflection ρ at the inner surface of the glass cell, the light is also refracted at the air/glass interface upon entering the prism, and also at the glass/air interface upon exiting the prism (see Fig. 2). Therefore, the additional contribution to the polarization change of the light must be taken into account. The total measured reflection coefficient ρ_{exp} is related to ρ through

$$\rho_{exp} = \frac{t_p^{ag}}{t_s^{ag}} \cdot \rho \cdot \frac{t_p^{ga}}{t_s^{ga}} \tag{2}$$

where $t_{p,s}^{ag}$ and $t_{p,s}^{ag}$ are the Fresnel transmission coefficients at the air/glass and glass/air interface, respectively, for parallel and perpendicular polarized light.

Considering the air/glass and glass/air interfaces, Eq. (2) can be rewritten to

$$\rho_{exp} = \frac{1}{\cos(\theta_a - \theta_g)} \cdot \rho \cdot \frac{1}{\cos(\theta_g - \theta_a)} = \frac{\rho}{\cos^2(\theta_a - \theta_g)} \tag{3}$$

in which $\theta_a = 45°$ (defined by the 90° top angle of the prism) and θ_g are the incident and refracted angles, respectively, with respect to the normal of the short sides of the prism. The incident angle θ_0 on the inner surface of the glass cell is given by $\theta_0 = 45° + \theta_g$. The angle θ_g is related to θ_a through Snell's law. Since θ_g depends on the refractive index of the prism, and the latter is a function of the photon energy of the light, the incident angle θ_0 also varies slightly with the photon energy. Using the refractive index of BK7 optical glass, we find that the effective incident angle θ_0 decreases from 72.92° to 72.37° between 1.5 eV and 3.5 eV. Now that we know the wavelength-dependent refraction angle in the prism, the correction factor $\cos^2(\theta_a - \theta_g)$ in Eq. (3) can be calculated as a function of photon energy. Since the BK7 glass is transparent over the entire measured photon energy range (0.8–3.5 eV), the refraction angle θ_g, and consequently also the correction factor, is a real, non-complex quantity. Therefore, the correction factor only influences the experimentally determined value of Ψ.

2.4. Principal component analysis

Ellipsometry spectra recorded during adsorption are analyzed using a principal component analysis (PCA). As demonstrated previously [26], PCA is a statistical technique that allows us to analyze a set of spectra without optical modeling. Summarizing our previous work, a set of spectra of gold nanoparticles deposited on a substrate can be represented by a single principal component and the corresponding coefficient

$$\frac{\rho_i}{\rho_0} - 1 \approx c_i Y \tag{4}$$

In this equation ρ_i is the ith spectrum of the set, ρ_0 is the spectrum of the substrate before deposition. Y is the principal component of the set, and c_i is the coefficient for the ith spectrum. Once the components are known, every spectrum of the set is completely characterized by the value of the coefficient c_i. This number is closely related to the coverage of the substrate with particles and is therefore used as the coverage measured in arbitrary units. In this way, trends in the ellipsometry spectra can be conveniently extracted from the measurements, which is sufficient for the investigation of the influence of the applied voltage or other parameters on the deposition process. If real quantitative information has to be obtained from the spectra, a calibration can be applied. A much more extensive discussion on PCA and its application to ellipsometry spectra is presented elsewhere [26].

3. Results

3.1. Field assisted deposition

To study the process of nanoparticle deposition and the effect of an electric field, we performed a quasi-static experiment in which the applied potential is decreased to more negative values in small steps. The current through the cell is measured and ellipsometry spectra are simultaneously recorded. The results are shown in Fig. 3.

Initially, an open circuit potential of approximately +0.2 V is measured. After 42 min the voltage was switched to −0.35 V. Subsequently, the potential is decreased in 0.1 V steps every 35 min, until a voltage of −0.85 V is

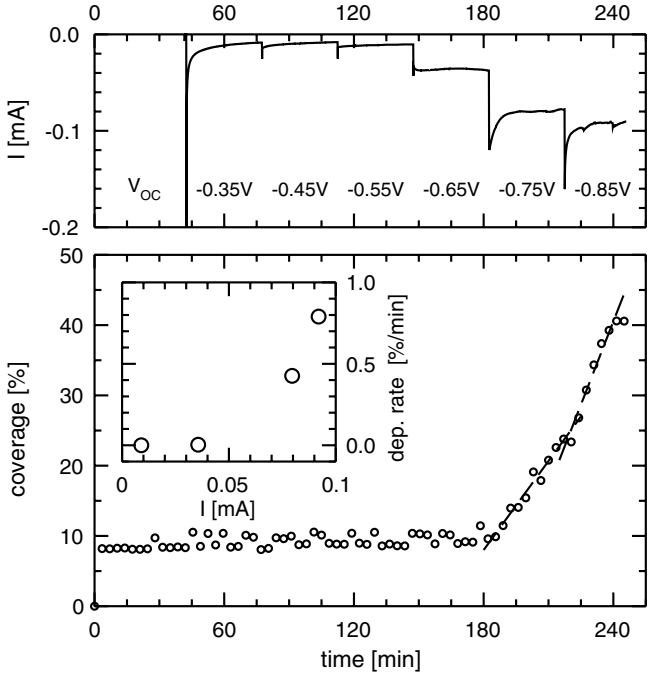

Fig. 3. Electric field induced deposition of gold nanoparticles. Initially, the potential is equal to the open circuit potential. Subsequently, the applied potential is varied from −0.35 V to −0.85 V in steps of 0.1 V. The upper figure shows the current as a function of time. The moments at which the potential is made more negative are clearly visible. The lower figure shows the particle coverage on the substrate. The data show that for deposition to take place, the potential is required to be more negative than a threshold value. In the inset, the dependence of the deposition rate on the current is shown.

reached. The moments at which the potential is changed are clearly observed in the current (upper part of Fig. 3). Upon changing the potential, the current exhibits a distinct peak due to charging of the electrical double layer at the surface. More importantly, no significant, continuous current is observed as long as the potential is more positive than −0.65 V. At more negative potentials, the magnitude of the current increases. Based on cyclic voltammetry experiments, the current is ascribed to the reduction of benzoate species, since hydrogen evolution only occurs at potentials more negative than approximately −1.1 V.

In the lower graph of Fig. 3, the time-dependence of the surface coverage is shown. The coverage is obtained from the simultaneously measured ellipsometry spectra. Analysis of the spectra using PCA yields a quantity that is proportional to the surface coverage. To obtain an absolute surface density of particles, the PCA results are calibrated using scanning electron microscopy (SEM) on the sample after the deposition experiment. An example of such an SEM image corresponding to the experiment in Fig. 3 is shown in Fig. 4 (left). Further details pertaining to the morphological characterization of the deposited layers will be discussed in the following section.

At the start of the experiment in Fig. 3, the first points already deviate markedly from zero, suggesting a fast initial deposition process, even before the first ellipsometry spectrum is obtained. To verify that this signal indeed is due to adsorbed particles, we inspected the actual ellipsometry spectra obtained in the initial stages of the experiment. Spectra measured during the first few minutes already exhibit a feature near 2.4 eV, which can be ascribed to the surface plasmon resonance of the gold nanoparticles. This indicates that indeed particles are adsorbed in a rapid pre-deposition process as soon as the suspension is inserted in the cell. Possibly, the substrate has obtained a negative charge due to oxidation of the surface during mounting of the sample and initial alignment and calibration procedures. The thus induced attractive particle-substrate interaction, combined with the efficient transport of nanoparticles toward the surface upon injection of the liquid, gives rise to a rapid pre-deposition.

After the initial adsorption, the surface coverage increases only very slowly, even when a potential as negative as −0.65 V is applied. As mentioned above, at these voltages no significant current is observed, which implies that the applied potential is shielded by the electrical double layer at the electrode. Consequently, there is no electric field in the bulk of the suspension, and particles do not experience a net driving force toward the surface of the electrode. Only particles that diffuse into the double layer are sensitive to an electric field, and will be adsorbed at the electrode. Still, at potentials as negative as −0.65 V, a much faster film growth can be expected. However, it has been reported that the double layer potential of a gold electrode in contact with an aqueous electrolyte is considerably smaller than the externally applied potential [27]. Upon applying a potential, hydroxyl groups at the gold surface accept or donate a proton, therewith reducing the double layer potential. The reduction of the double layer potential also depends on the acidity (pH) of the solution but is typically 85–90%, therewith explaining the low deposition rate in our experiments. When the voltage is stepped to −0.75 V, the lower part of Fig. 3 reveals that adsorption starts immediately. A subsequent 0.1 V step of the applied potential leads to an increase of the deposition rate by a factor of 1.9. Apparently, there is a threshold for deposition to be initiated. Its value is generally found to be between −0.65 V and −0.75 V, which corresponds quite well with the threshold of approximately −0.65 V for current flow, observed in the upper graph of Fig. 3. From this observation we conclude that the deposition rate is closely related to the current flowing through the cell.

In Fig. 5 the result of a second field assisted adsorption experiment is shown. As with the previous measurement, the absolute surface coverage has been obtained from the ellipsometry spectra by calibration of the relative PCA results using the SEM image in Fig. 4 (right). Approximately 20 min after the start of the experiment, the poten-

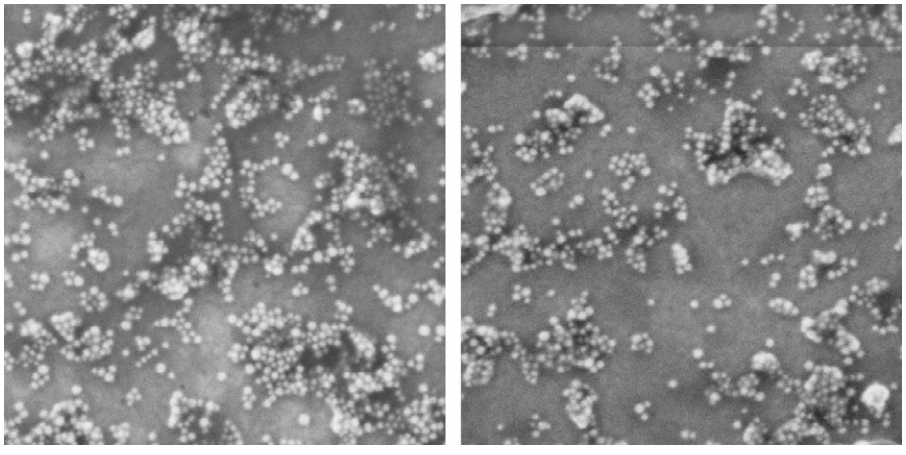

Fig. 4. Scanning electron microscopy images of nanocolloidal gold films deposited in the presence of an external electric field. Depicted is the morphology after the deposition experiments shown in Figs. 3 (left) and 5 (right). The coverages amount to 41% and 9%, respectively.

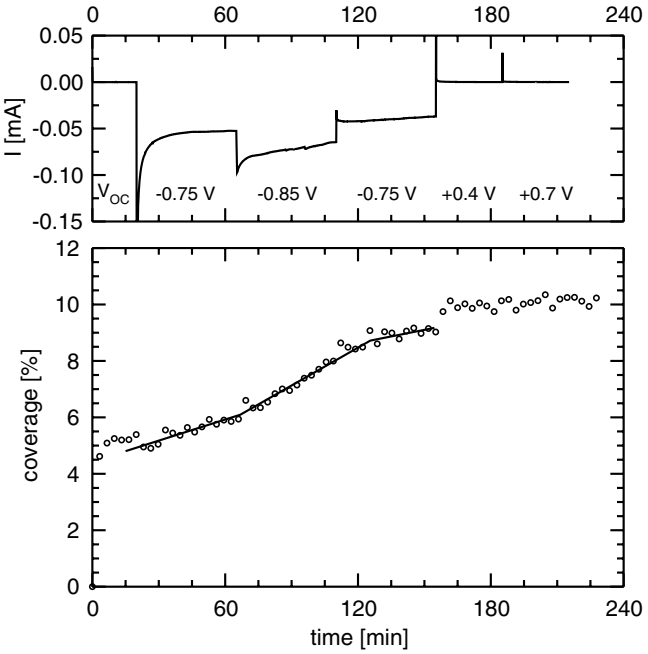

Fig. 5. Electric field assisted deposition experiment showing the influence of the applied voltage on the deposition rate, and the irreversibility of the adsorption. The upper graph shows the current as a function of the applied potential. In the lower graph the development of surface coverage is shown. The values of the applied voltage are indicated in the upper graph.

tial is stepped from the open circuit value to −0.75 V. Subsequently, after 45 min, the negative potential is further increased to −0.85 V, and stepped back after another 45 min. Upon changing the voltage to −0.85 V, the deposition rate is increased by a factor of 1.8, in good agreement with the factor of 1.9 observed in the previous experiment. After switching the voltage back to −0.75 V, the deposition rate decreases again to a value that is approximately equal to the initial value.

Comparison of Figs. 3 and 5 reveals that, despite the relative similarities mentioned above, the absolute deposition rates differ by approximately one order of magnitude. Also, the initially deposited nanoparticle density is 50% lower in Fig. 5. Generally, when comparing several similar experiments, often such marked differences are observed. Although the precise cause of these discrepancies is unclear, we assume them to be due small variations of the surface charge on the particles in various experiments, either arising from slightly different synthesis conditions or ionic strengths of the particle suspensions. If the variations are limited, both the ionic strength and the particle surface charge do not influence the electrochemical processes, i.e. the absolute current observed. However, the effective electrophoretic force on the particles is strongly dependent on these quantities.

After the adsorption of the gold nanoparticles in the presence of an electric field, we attempted to desorb the particles by reversing the applied potential. Upon switching the voltage to +0.4 V, an instantaneous increase in the optical signal is observed, giving rise to an apparent 1% step in the effective surface coverage (lower part of Fig. 5). We attribute this change to electroreflection, a change of the dielectric properties of a metal due to modification of the electron density at the electrode surface, which is in turn caused by an applied voltage. After this change we do not observe a decrease of the coverage, not even when the voltage is increased to +0.7 V. This experimental observation deviates from the results of Giersig and Mulvaney [19]. They conclude that desorption of particles occurs when the applied potential is reversed. An explanation for the difference between their and our experiments may be sought in terms of the Van der Waals forces between particles and substrate. In their case, these forces are much smaller since they use a carbon coated copper grid as substrate whereas we have a metallic substrate. Therefore, in our situation the particles are expected to be more strongly bound to the electrode. Their immobility inhibits the formation of large ordered domains in the colloidal films.

3.2. Film morphology

To investigate the morphology of the nanocolloidal films, deposited in the presence of an external electric field, the samples are removed from the deposition cell, carefully rinsed and dried. Subsequently, electron microscopy (SEM) is used to study the spatial distribution of the nanoparticles. Images obtained after the deposition experiments in Figs. 3 and 5 are shown in Fig. 4. In both experiments a very similar spatial distribution is observed. When comparing the present results with irreversibly deposited nanoparticle layers on chemically functionalized surfaces [4,5,28], a number of important differences are discerned. First, the spatial distribution of particles deposited under the influence of an electric field is considerably more inhomogeneous. Clusters of 20–50 particles coexist with relatively large areas without particles. Close inspection reveals that some of the clusters show some azimuthal order. These observations indicate the presence of a long-ranged attractive force between the particles. The second observation is that in several locations on the surface, a second layer is adsorbed. The pictures also show some dark spots in the image. These are probably due to organic pollution of the dried samples, most likely originating from the benzoic acid buffer.

To enable a more quantitative comparison between the films deposited using a chemically modified substrate [4,5,28] and those made by electric field assisted deposition, the two-dimensional radial distribution function of a film deposited in the presence of an electric field is calculated. The radial distribution function $g(r)$ expresses the probability to find a particle at a distance r from another particle [4]. Unfortunately, the nanoparticulate films in Fig. 4 exhibit a number of particles in a second layer, these are not suitable for the calculation of a two-dimensional radial distribution function.

Using a less negative deposition voltage of −0.75 V, the coverage is markedly lower and particles are primarily distributed in a single layer. A typical image is shown in Fig. 6. The two-dimensional autocorrelation function (inset in Fig. 6) is calculated from the manually determined particle centers of all particles. This approach has the advantage that the convolution with the particle size is eliminated, rendering the autocorrelation image much sharper. The radial distribution function is calculated by evaluating all particle–particle distances. The calculated distribution function is normalized using the requirement that its value should be one at infinity and is plotted as a function of the distance divided by the position of the first maximum r_0. The result is shown in the lower part of Fig. 6.

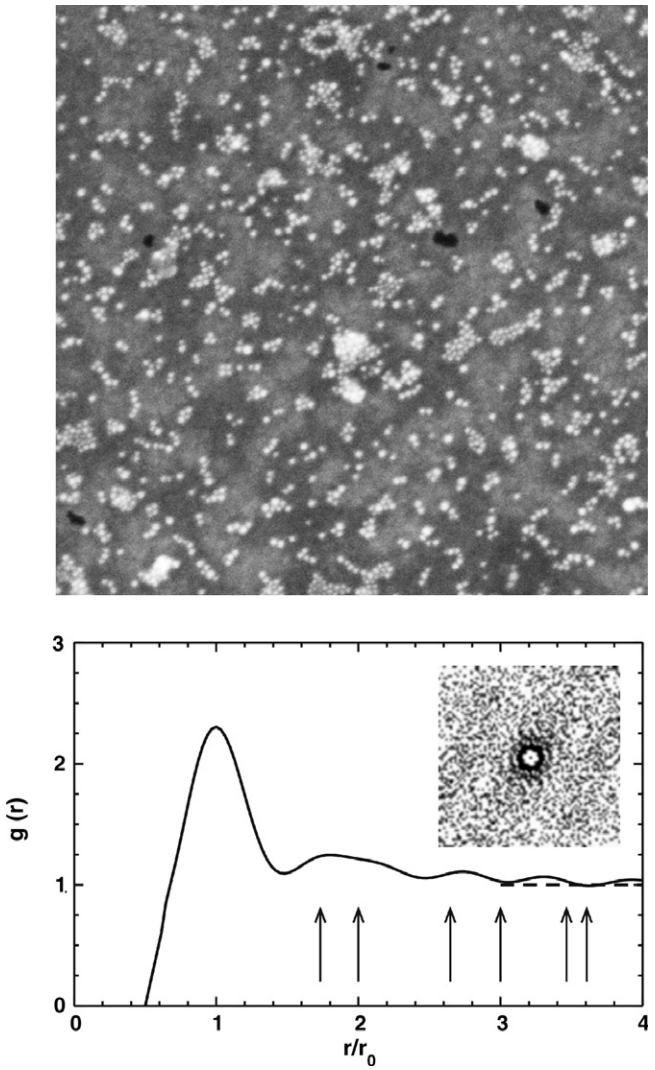

Fig. 6. Scanning electron microscopy image after electric field assisted gold nanoparticle deposition at −0.75 V for 250 min (top) and the radial distribution function calculated from this image (bottom). The radial distribution function $g(r)$ is plotted as a function of r/r_0, where $r_0 = 10.9$ nm is the average minimum particle–particle distance. The dashed line represents the large distance limit. Positions where peaks are expected for perfect hexagonal order are indicated by arrows. The inset shows the two-dimensional autocorrelation function of the particle distribution.

The position $r_0 = 10.9$ nm of the first maximum reflects the nearest-neighbour distances observed in the SEM images. From the TEM experiment (Fig. 1), the diameter of the metallic nanoparticles was determined at 8.6 nm, implying that the surface-to-surface interparticle separation is 2.3 nm. Since the length of the octadecylamine molecule on the surface of the gold nanoparticles amounts to approximately 1.5 nm, this means that the interparticle gap is 24% smaller than twice the length of the stabilising molecule. Giersig and Mulvaney noticed a similar phenomenon for larger gold particles stabilised with different thiols [19]. It is ascribed to intertwining of the stabilizing molecules.

At distances up to four nearest-neighbour separation lengths, more maxima are observed, indicating that radial ordering persists up to a distance of a few particle diameters. The height of these peaks is progressively lower since the number of larger clusters becomes smaller. In Fig. 6, the theoretical peak positions for a perfectly hexagonal lattice are indicated by arrows. It is clear that the observed peak positions do not match with the calculated distances. This demonstrates that the azimuthal correlation is lost at larger distances, probably owing to the fact that the particles are relatively strongly bound to the surface.

4. Discussion

The correspondence between nanoparticle deposition and electrochemical current, as observed in Figs. 3 and 5, appears to indicate that the reduction reaction at the working electrode provides a driving force for deposition. A simple model, schematically represented in Fig. 7, may explain the experimental findings.

At low voltages, below the aforementioned threshold value, the applied potential is completely shielded by the double layer formed at the electrode surface. Consequently, there is no net field in the bulk of the suspension at distances from the electrode surface exceeding the spatial extent of this double layer, i.e. the Debye length. In this situation, shown in the left part of Fig. 7, only particles which approach the electrode within the Debye length will experience an attractive force, and a very low, negligible adsorption rate is expected.

Upon applying larger negative voltages, the reduction of species at the electrode locally creates excess negative space charge. Diffusion and Coulombic repulsion will lead to distribution of the charge throughout the bulk of the suspension. At large distances from the electrode, the charge is compensated by that generated at the counter electrode, therewith maintaining a constant net flow of charge in the electrolyte solution. The charge distribution constitutes a field gradient with a large spatial extent compared to the Debye length, providing a migration force on the suspended particles. This situation is depicted in the right part of Fig. 7. Quinn et al. [29] use a very similar mechanism to

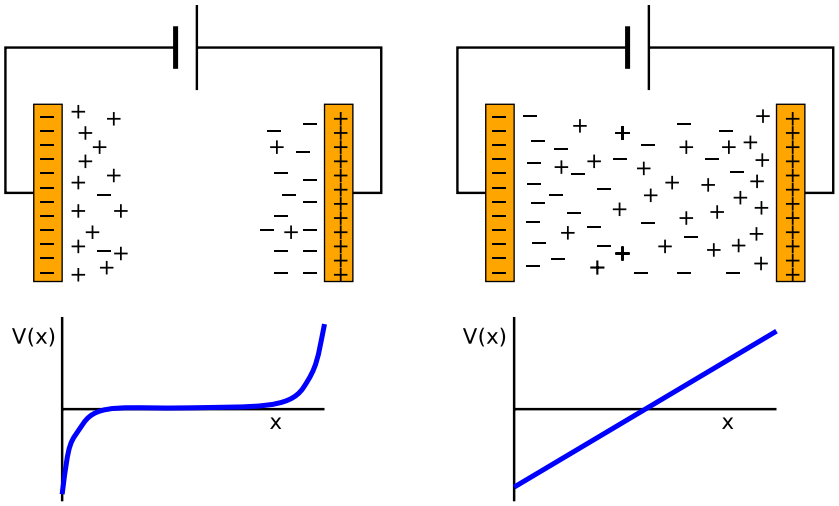

Fig. 7. Schematic representation of the charge distribution in the cell and the resulting potential distribution. The left and the right figures depict the situation in the absence and in the presence of an electrochemical current, respectively, arising from the applied potential.

analyze the particle flux toward an electrode. In their experiments, they electrochemically detect electrophoretically deposited latex beads on a gold micro-electrode. In our model, the transition between the two situations sketched in Fig. 7 corresponds to the threshold value of approximately −0.75 V. The model may also account for the observation in Fig. 3 that at −0.65 V current is already detected while deposition does not occur. Apparently, the electric field is not sufficiently strong to overcome the Brownian motion of the nanoparticles in suspension.

In the above discussion, only the migration of the particles toward the substrate is considered. The question which remains to be answered is: What happens at the surface? As described in the previous section, the nanoparticle clusters exhibit a short-range order. To induce an ordering process, a long-range attractive particle–particle interaction needs to be present. Two possible candidates for such forces are (i) electrohydrodynamic forces occurring during the adsorption process, or (ii) capillary forces acting upon drying of the deposited layers. Since most particles appear to be in a monolayered structure, we discard the possibility of cluster formation in the suspension prior to deposition.

Electrohydrodynamic forces have been described to give rise to the formation of hexagonally ordered clusters and extended monolayers of much larger particles at electrode surfaces [8,11–13]. In these cases the clusters are imaged by in situ optical microscopy, so drying effects do not play a role. In our experiments this is uncertain, because SEM images are obtained after drying of the layers. To estimate the contribution of capillary forces, we performed a deposition experiment without applied field, i.e. in the absence of electrohydrodynamic. A gold substrate is cleaned in a piranha solution, after which the surface is not reduced thus leaving it negatively charged. Subsequently, the sample is rinsed and immediately immersed in a nanocolloidal gold suspension with an identical composition as used for the field assisted experiments.

After removal from the colloidal suspension, the SEM image shown in Fig. 8 is obtained. The attractive interaction between the surface and the positively charged nanoparticles indeed gives rise to adsorption of a small number of gold particles. In fact, this low density of nanoparticles adsorbed even in the absence of an applied potential is in agreement with the initial deposition observed in Figs. 3 and 5. Only qualitative proof can be given by this method, since removal of the sample from the suspension gives rise to detachment of an unknown fraction of the particles as they are only electrostatically, i.e. not chemically bound to the surface.

Most of the gold nanoparticles in Fig. 8 appear as monomers, while only a few small clusters, mostly dimers, are observed. Since the number of particles on the surface is relatively small, capillary forces are absent on large parts of the surface. These only come into play when particles are

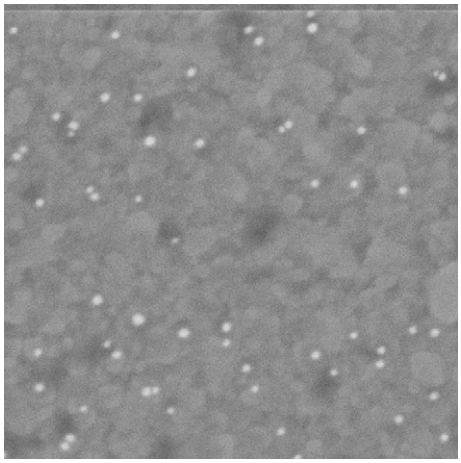

Fig. 8. Scanning electron microscopy image after immersion of a negatively charged (not reduced) substrate into the nanocolloidal gold suspension for typically 1 h, without an applied electric field.

close together. Since the few clusters still exhibit an interparticle distance which is on average markedly larger than for the field assisted deposited layers, this suggests that capillary forces may have a small contribution to the formation of the films, but that they are not predominant. Therefore, primarily electrohydrodynamic flow induced interactions are considered to be responsible for the formation of the clusters observed in Fig. 4.

5. Conclusions

Nanocolloidal gold particles are deposited from an aqueous benzoate/benzoic acid solution at metal-coated glass substrates, in the presence of an externally applied electric field. A relatively high, positive surface charge originates from the octadecylamine stabilizing agent on the nanoparticle surfaces, and enables electric field assisted deposition at negative potentials.

The mechanism governing the deposition process is investigated by studying the influence of the applied potential. At low voltages, the current is negligible and deposition does not occur. At higher voltages, a strong increase in both the current and the deposition rate is observed. We propose a mechanism in which the larger polarization of the electrode results in the electrochemical reduction of the benzoic acid. This reaction gives rise to a net space charge in the suspension, therewith constituting an electric field that extends through the entire cell. This field provides the driving force for deposition of the nanoparticles. Variations of the deposition rate in different experiments is ascribed to slight differences of either the surface charge of the particles and/or the ionic strength of the suspension.

The spatial distribution of the nanoparticles within the adsorbed layers, formed by field assisted deposition, exhibit significant clustering, which suggests the influence of a long-ranged attractive force. Although capillary forces play a role during drying of the film, electrohydrodynamic flow is the most important interaction. The radial distribution function, determined from ex situ electron microscopy images, shows that the degree of order at the surface is markedly improved as compared to randomly deposited nanocolloidal films at chemically derivatized surfaces. In addition to the enhanced radial order within the film, the clusters also reveal a limited degree of azimuthal ordering.

Acknowledgements

We thank M.P.B. van Bruggen and A. van Silfhout for helpful discussions. This work is part of the research program of the Stichting voor Fundamenteel Onderzoek der Materie (FOM), financially supported by the Nederlandse Organisatie voor Wetenschappelijk Onderzoek (NWO) and Philips Research.

References

[1] C.B. Murray, C.R. Kagan, M.G. Bawendi, Annu. Rev. Mater. Sci. 20 (2000) 545–610.
[2] F. Caruso (Ed.), Colloids and Colloid Assemblies, Wiley-VCH, 2004.
[3] M.P. Pileni (Ed.), Nanocrystals Forming Mesoscopic Structures, Wiley-VCH, 2005.
[4] E.S. Kooij, E.A.M. Brouwer, H. Wormeester, B. Poelsema, Langmuir 18 (2002) 7677–7682.
[5] E.A.M. Brouwer, E.S. Kooij, H. Wormeester, B. Poelsema, Langmuir 19 (2003) 8102–8108.
[6] M. Trau, D.A. Saville, I.A. Aksay, Science 272 (1996) 706–709.
[7] M. Böhmer, Langmuir 12 (1996) 5747–5750.
[8] M. Trau, D.A. Saville, I.A. Aksay, Langmuir 13 (1997) 6375–6381.
[9] A.L. Rogach, N.A. Kotov, D.S. Koktysh, J.W. Ostrander, G.A. Ragoisha, Chem. Mater. 12 (2000) 2721–2726.
[10] Z.-Z. Gu, S. Hayami, S. Kubo, Q.-B. Meng, Y. Einaga, D.A. Tryk, A. Fujishima, O. Sato, J. Am. Chem. Soc. 123 (2001) 175–176.
[11] W.D. Ristenpart, I.A. Aksay, D.A. Saville, Phys. Rev. Lett. 90 (2003) 128303.
[12] P.J. Sides, Langmuir 17 (2001) 5791–5800.
[13] W. Ristenpart, I.A. Aksay, D.A. Saville, Phys. Rev. E 69 (2004) 021405.
[14] J.A. Fagan, P.J. Sides, D.C. Prieve, Langmuir 20 (2004) 4823–4834.
[15] J.A. Fagan, P.J. Sides, D.C. Prieve, Langmuir 21 (2005) 1784–1794.
[16] P.J. Sides, Langmuir 19 (2003) 2745–2751.
[17] R.C. Bailey, K.J. Stevenson, J.T. Hupp, Adv. Mater. 12 (2000) 1930–1934.
[18] M. Gao, J. Sun, E. Dulkeith, N. Gaponik, U. Lemmer, J. Feldmann, Langmuir 18 (2002) 4098–4102.
[19] M. Giersig, P. Mulvaney, Langmuir 9 (1993) 3408–3413.
[20] O.D. Velev, K.H. Bhatt, Soft Matter 2 (2006) 738.
[21] R.M.A. Azzam, N.M. Bashara, Ellipsometry and Polarized Light, second ed., North-Holland, Amsterdam, 1987.
[22] H.G. Tompkins, W.A. McGahan, Spectroscopic Ellipsometry and Reflectometry: A User's Guide, John Wiley & Sons Inc., New York, 1999.
[23] M. Aslam, L. Fu, M. Su, K. Vijayamohanan, V.P. Dravid, J. Mat. Chem. 14 (2004) 1795–1997.
[24] J.M.M. de Nijs, A.H.M. Holtslag, A. Hoekstra, A. van Silfhout, J. Opt. Soc. Am. A 5 (1988) 1466–1471.
[25] J.M.M. de Nijs, Ellipsometry and the Ti/c-Si solid state reaction, Ph.D. thesis, University of Twente (1989).
[26] E.A.M. Brouwer, E.S. Kooij, H. Wormeester, M.A. Hempenius, B. Poelsema, J. Phys. Chem. B 108 (2004) 7748–7753.
[27] D. Barten, J.M. Kleijn, J. Duval, H.P. van Leeuwen, L. Lyklema, M.A. Cohen Stuart, Langmuir 19 (2003) 1133–1139.
[28] A.A. Mewe, E.S. Kooij, B. Poelsema, Langmuir 22 (2006) 5584.
[29] B.M. Quinn, P.G. van't Hof, S.G. Lemay, J. Am. Chem. Soc. 126 (2004) 8360–8361.